Geofísica Internacional
ISSN: 0016-7169
silvia@geofisica.unam.mx
Universidad Nacional Autónoma de México
México

Gamio, J. C.; Ortiz-Alemán, C.; Martin, R.
Electrical capacitance tomography two-phase oil-gas pipe flow imaging by the linear back-projection algorithm
Geofísica Internacional, vol. 44, núm. 3, july-september, 2005, pp. 265-273
Universidad Nacional Autónoma de México
Distrito Federal, México

Geofísica Internacional (2005), Vol. 44, No. 3, pp. 265-273

Electrical capacitance tomography two-phase oil-gas pipe flow imaging by the linear back-projection algorithm

J. C. Gamio, C. Ortiz-Alemán and R. Martin
Instituto Mexicano del Petróleo, México, D. F., México

Received: August 5, 2004; accepted: December 7, 2004

RESUMEN

La Tomografía de Capacitancia Eléctrica (TCE) es una nueva tecnología capaz de lidiar con la complejidad de la medición de flujos bifásicos de gas-aceite, derivando la distribución de componentes en dos planos adyacentes a lo largo de un ducto. Una de sus aplicaciones más prometedoras es la visualización de flujos de gas y aceite. TCE ofrece algunas ventajas sobre otras modalidades tomográficas: no hay radiación, una respuesta rápida, bajo costo, es una técnica no intrusiva y no invasiva, y la posibilidad de operar con altas temperaturas y altas presiones. El método denominado "linear back-projection (LBP)" es una de las técnicas más populares que se emplean en la reconstrucción de imágenes a partir de datos de tomografía de capacitancia eléctrica. A pesar de su pobre exactitud, es un procedimiento simple y rápido capaz de operar en tiempo real en muchas aplicaciones y ha permanecido como una opción muy popular. Sin embargo, desde que fue propuesto por vez primera ha carecido de un suporte formal, en el contexto de esta aplicación. Su única justificación radica en que es una adaptación de un método comúnmente empleado en la tomografía médica de rayos X, así como en el hecho de que produce imágenes útiles (aunque sólo "cualitativamente" buenas). En este trabajo se presenta una forma ilustrativa de interpretar el método LBP. Se muestra cómo el método LBP está basado en la linealización de una forma normalizada del problema directo. Más específicamente, el problema directo normalizado se aproxima mediante una serie de hiperplanos. La matriz de reconstrucción utilizada en el método LBP resulta ser una transpuesta "ponderada" del operador lineal (matriz) que define el problema directo normalizado. Los renglones de esta última matriz contienen la información de los mapas de sensitividades empleados en el método LBP.

PALABRAS CLAVE: Tomografía de capacitancia, reconstrucción de imágenes, visualización de flujos, modelado inverso.

ABSTRACT

Electrical Capacitance Tomography (ECT) is a novel technology that can deal with the complexity of two-phase gas-oil flow measurement by explicitly deriving the component distributions on two adjacent planes along a pipeline. One of its most promising applications is the visualization of gas-oil flows. ECT offers some advantages over other tomography modalities, such as no radiation, rapid response, low-cost, being non-intrusive and non-invasive, and the ability to withstand high temperature and high pressure. The linear back-projection (LBP) algorithm is one of the most popular methods employed to perform image reconstruction in ECT. Despite its relatively poor accuracy, it is a simple and fast procedure capable of real-time operation in many applications, and it has remained a very popular choice. However, since it was first reported it has lacked a clear formal support in the context of this application. Its only justification has been that it was an adaptation of a method normally used in linear X-ray medical tomography, and the fact that it actually does produce useful (albeit only 'qualitative') images. In this paper, one illustrative way of interpreting LBP is presented. It is shown how LBP is actually based on the linearisation of a normalised form of the forward problem. More specifically, the normalised forward problem is approximated by means of a series of hyper-planes. The reconstruction matrix used in LBP is found to be a 'weighted' transpose of the linear operator (matrix) that defines the linearised normalised forward problem. The rows of this latter matrix contain the information of the sensitivity maps used in LBP.

KEY WORDS: Capacitance tomography, linear back-projection, image reconstruction, flow imaging, inverse modelling.

1. INTRODUCTION

It is important to measure the fluids produced from oil wells accurately for efficient oil exploitation. Typically, field wells produce a complex mixture of gas, oil, water and other components, such as sand, and it is difficult to estimate the multi-phase flow relative composition. The conventional approach is to separate the mixture into individual components, and then measure those separately using single-phase flow meters, *e.g*. orifice plates for gas and turbine meters for oil. There are some problems with the required separators: bulky, high installation cost and considerable maintenance. Therefore, it is highly attractive to have relatively simple multiphase flow meters, which are capable of measuring the flow rate of each component directly, without separation.

Electrical capacitance tomography (ECT) is an imaging technique suitable for industrial processes involving nonconducting mixtures such as gas-oil (Xie *et al*., 1989; Xie *et al*., 1992; Yang *et al*., 1995). The basic principle of ECT is to

use a sensor (Figure 1) made of a ring of n adjacent rectangular electrodes (separated by small gaps) placed around a non-conducting pipe or vessel, which contains the process fluids or materials. To avoid external interference, the sensor also includes two grounded cylindrical end guards, and an exterior grounded metallic screen covering the whole assembly. All the inter-electrode mutual capacitances are measured, corresponding to the $\frac{1}{2}\,n\,(n\text{-}1)$ different electrode pairs. The values of the self and mutual capacitances are found by applying known potentials to the sensor electrodes and measuring the electrode charges. In practice, the determination of the electrode charges is normally done indirectly by measuring the electrode currents, and the excitation potentials are applied to the electrodes in the form of a periodic signal of known amplitude. The 12-electrode ECT system employed for this study makes use of a single-electrode excitation method. With this method, the mutual capacitances are determined as follows: first an excitation voltage is applied to electrode 1 while keeping all the others at zero potential and the charge on electrodes 2 to 12 is measured; next, the excitation voltage is applied to electrode 2 while keeping all the others at zero and the charge on electrodes 3 to 12 is measured. This procedure is repeated until voltage is applied to electrode 11 and the charge of electrode 12 is measured. In this way, 66 independent mutual capacitance values are determined.

The measured capacitances are non-linear functions of the unknown relative-electrical-permittivity (henceforth permittivity for short) distribution inside the sensor. From the measured data and using a suitable reconstruction algorithm, an image is obtained of the permittivity distribution $\varepsilon(x, y)$ at the cross-section defined by the electrode ring, which reflects the mixture component distribution.

There are several algorithms for ECT image reconstruction (Isaksen, 1996; Yang and Peng, 2003; Ortiz-Alemán *et al*., 2004), but linear back-projection (LBP) (Xie *et al*., 1989; Xie *et al*., 1992) is the simplest and fastest one. In the following sections, first the LBP algorithm is briefly described and then an intuitive interpretation is provided regarding how it actually works (what it does).

2. IMAGE RECONSTRUCTION USING LINEAR BACK-PROJECTION

The LBP algorithm is a simple procedure for reconstructing an image of an unknown permittivity distribution inside the sensor from the capacitance measurements. It was one of the first algorithms used for this purpose and is still very commonly employed, despite the development of a number of other methods (Isaksen, 1996; Yang, 2003; Ortiz-Alemán *et al*., 2004). Although its reconstruction accuracy is not very good, LBP has the advantage of being quite fast, in practice requiring only the multiplication of a fixed reconstruction matrix times the vector of measurements. In principle, LBP can be viewed as a weighted back-project or 'smearing' of each one of the normalised measurements along its sensing zone, given by the corresponding sensitivity map. However, since this algorithm was first introduced by Xie *et al*. in two papers back in 1989 and 1992, it has lacked any clear mathematical support. Its only justification has been that it was an adaptation of a method normally used in linear X-ray medical tomography, and the fact that it actually does produce useful (albeit only 'qualitative') images.

Let us consider an n-electrode sensor and an image made of p equal-area regions or pixels located inside the pipe. For each one of the $m=\frac{1}{2}n\,(n\text{-}1)$ possible electrode-pair combinations, a capacitance sensitivity map can be defined by

$$s_i(k) = \frac{c_i(k) - c_{i\ (emp)}}{c_{i\ (full)} - c_{i\ (emp)}} \quad \text{for} \quad i = 1, \ldots, m\,, \qquad (1)$$

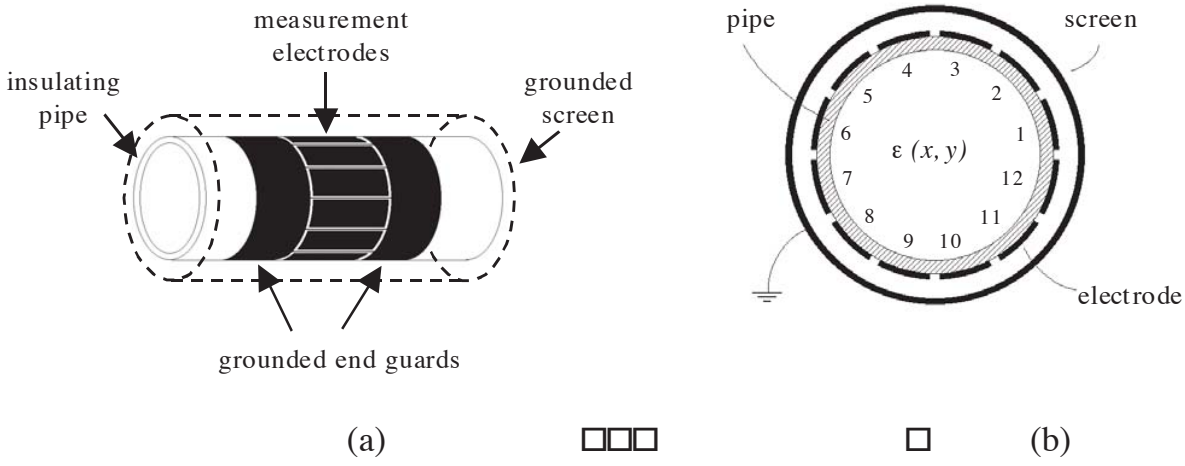

Fig. 1. ECT sensor: (a) whole assembly and (b) cross-section.

where k is the pixel number (from 1 to p), c_i (k) is the capacitance measured with electrode pair i when the area of pixel k is full of the higher-permittivity material while the rest of the sensor is full of the lower-permittivity material, whereas $c_{i(full)}$ and $c_{i(emp)}$ are the capacitances for electrode pair i when the sensor is full of high- and low-permittivity material, respectively. These sensitivity maps were calculated by using a 2D finite volume model of the sensor. The sensitivity maps, as computed in this work, represent a normalized approximation to the first order of the partial derivative of the capacitance data with respect to the parameters (see equations 10, 11, and 12).

Prior to back-projection, the raw capacitance measurements corresponding to each electrode pair i are normalised according to

$$\lambda_i = \frac{c_i - c_{i\ (emp)}}{c_{i\ (full)} - c_{i\ (emp)}}\ , \qquad (2)$$

where λ_i is the normalised capacitance for electrode pair i and c_i is the actual capacitance measured with that electrode pair.

The basic LBP formula (without thresholding or truncation) calculates a grey level $g(k)$ for each pixel as

$$g(k) = \frac{\sum_{i=1}^{m} \lambda_i\, s_i(k)}{\sum_{i=1}^{m} s_i(k)} \quad \text{for} \quad k = 1, \ldots, p\ . \qquad (3)$$

This grey level is supposed to be linearly related to the permittivity, with g=0 and g=1 corresponding to the permittivities of the low- and high-permittivity materials, respectively. The actual back-projection operation occurs in the numerator of equation (3), while the quantity in the denominator serves as a position-dependent weighting factor used to compensate for the decrease in sensitivity towards the centre of the sensor. Note that the mathematical operation of equation (3) is equivalent to multiplying a reconstruction matrix **R** times the vector of normalised capacitance λ, *i.e.*

$$\mathbf{g} = \mathbf{R}\boldsymbol{\lambda}\ , \qquad (4)$$

where g is the $p \times 1$ vector of pixel grey levels, **R** is the $p \times m$ matrix whose columns are the sensitivity maps after their elements have been weighted by the sum of all maps, and λ is the $m \times 1$ vector of normalised capacitances.

3. LBP METHOD

3.1 The linearised normalised forward problem

It will be shown how LBP is actually based on the linearisation of the normalised forward problem, approximating it by means of a series of hyper-planes. The original unnormalised forward problem is

$$\mathbf{c} = \begin{bmatrix} c_1 \\ \mathtt{M} \\ c_m \end{bmatrix} = \mathbf{f}(\boldsymbol{\varepsilon}) = \begin{bmatrix} f_1(\boldsymbol{\varepsilon}) \\ \mathtt{M} \\ f_m(\boldsymbol{\varepsilon}) \end{bmatrix} \text{with } \boldsymbol{\varepsilon} = \begin{bmatrix} \varepsilon_1 \\ \mathtt{M} \\ \varepsilon_p \end{bmatrix}, \qquad (5)$$

where c is the vector of inter-electrode capacitance measurements, f_i are non-linear functions and ε is the vector of permittivities corresponding to the p pixels or regions in the sensing area. To normalise the problem, new variables (representing the image grey level g and the normalised capacitance measurements λ) must be introduced as follows:

$$g_i = \frac{\varepsilon_i - \varepsilon_{min}}{\varepsilon_{max} - \varepsilon_{min}} \quad \text{and} \quad \lambda_i = \frac{c_i - c_{i\ (emp)}}{c_{i\ (full)} - c_{i\ (emp)}}\ , \qquad (6)$$

where ε_{max} and ε_{max} are the upper and lower bounds of the permittivity (corresponding to the higher- and lower-permittivity materials). $c_{i\,(full)}$ and $c_{i\,(emp)}$ (defined in the previous section) are formally given as

$$c_{i(full)} = f_i(\boldsymbol{\varepsilon}_{\mathbf{max}}) \quad \text{and} \quad c_{i(emp)} = f_i(\boldsymbol{\varepsilon}_{\mathbf{min}})\ , \qquad (7)$$

where

$$\boldsymbol{\varepsilon}_{\mathbf{max}} = \begin{bmatrix} \varepsilon_{max} \\ \mathtt{M} \\ \varepsilon_{max} \end{bmatrix} \quad \text{and} \quad \boldsymbol{\varepsilon}_{\mathbf{min}} = \begin{bmatrix} \varepsilon_{min} \\ \mathtt{M} \\ \varepsilon_{min} \end{bmatrix}. \qquad (8)$$

Applying transformation (6), the full variation of g between $g_{min} = 0$ and $g_{max} = 1$ corresponds to a variation of ε between ε_{min} and ε_{max}. The normalised problems is the defined as

$$\boldsymbol{\lambda} = \begin{bmatrix} \lambda_1 \\ \mathtt{M} \\ \lambda_m \end{bmatrix} = \mathbf{h}(\mathbf{g}) = \begin{bmatrix} h_1(\mathbf{g}) \\ \mathtt{M} \\ h_m(\mathbf{g}) \end{bmatrix} \text{with } \mathbf{g} = \begin{bmatrix} g_1 \\ \mathtt{M} \\ g_p \end{bmatrix}, \qquad (9)$$

where h_i are still non-linear functions.

In (6) and (7) were defined λ_i and $c_{i(emp)}$, then it holds that $\boldsymbol{\lambda}\big|_{g=0} = \mathbf{h(0)} = \mathbf{0}$. Applying Taylor series and neglecting terms of order 2 and higher, **h** can be approximated in the vicinity of the origin ($\mathbf{g = 0}$) as

$$\boldsymbol{\lambda} = \mathbf{h}(\mathbf{g}) \approx \mathbf{S}\mathbf{g}\ , \qquad (10)$$

where **S** is the matrix of partial derivatives or Jacobian matrix (of size $m \times p$), evaluated at the origin:

$$\mathbf{S} = \left[s_{ij} \right] = \left[\left. \frac{\partial h_i}{\partial g_j} \right|_{g_j = 0} \right] \text{for } i = 1, \ldots, \text{m and } j = 1, \ldots, p \tag{11}$$

The elements of this Jacobian matrix can be approximated using finite differences as

$$s_{ij} = \frac{h_i(\mathbf{g_j}) - h_i(0)}{1 - 0} = \frac{h_i(\mathbf{g_j}) - 0}{1 - 0} = \frac{h_i(\mathbf{g_j})}{1} = h_i(\mathbf{g_j}) = \lambda_i\big|_{\mathbf{g_j}} \tag{12}$$

where $\mathbf{g_j} = \mathbf{u}_j$ is a unit vector having all its components equal to zero except the j-th, which is equal to one. This corresponds to a vector ε_j having all its components equal to ε_{min} except the j-th, which should be equal to ε_{max}. Therefore, from (6) and (12) we have

$$s_{ij} = \lambda_i\big|_{\mathbf{g_j}} = \lambda_i\big|_{\boldsymbol{\varepsilon}_j} = \frac{c_i\big|_{\boldsymbol{\varepsilon}_j} - c_{i(emp)}}{c_{i(full)} - c_{i(emp)}} = \frac{f_i(\boldsymbol{\varepsilon}_j) - f_i(\boldsymbol{\varepsilon}_{min})}{f_i(\boldsymbol{\varepsilon}_{max}) - f_i(\boldsymbol{\varepsilon}_{min})} . \tag{13}$$

In this way, to each function h_i corresponds a hyper-plane in a $(p+1)$-dimensional space, defined by the origin and the p points given by (13), with $1 \le j \le p$. Notice that various approximated rows of **S**, according to (13), contain what in LBP is known as the sensitivity maps (see Figure 2).

One problem with using the linear approximation (10) directly is that, albeit it will produce exact results for the points that define the hyper-planes (*i.e.*, the unit vectors $\mathbf{g}_j$), this will not for the vector $\mathbf{g}_{max}$ that corresponds to the sensor full happen of the high-permittivity material, defined as

$$\mathbf{g_{max}} = \begin{bmatrix} g_{max} \\ \text{M} \\ g_{max} \end{bmatrix} = \begin{bmatrix} 1 \\ \text{M} \\ 1 \end{bmatrix} \tag{14}$$

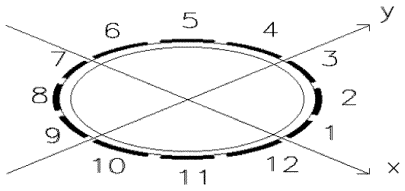

(a) Location of electrodes

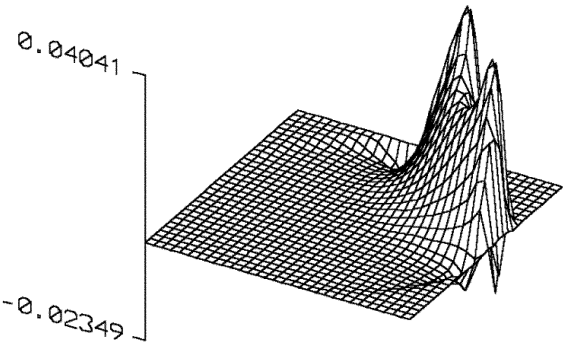

(b) S_{13}

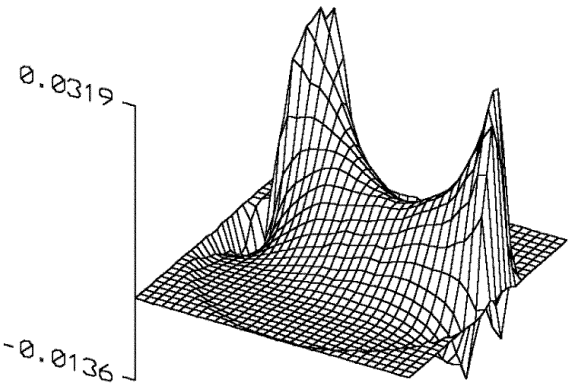

(c) S_{15}

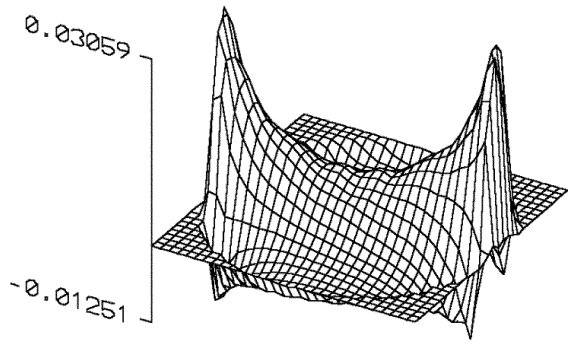

(d) S_{17}

Fig. 2 . Typical shapes of the sensitivity maps.

If this is deemed desirable, an additional re-normalisation can be introduced to ensure that

$$\boldsymbol{\lambda}\big|_{\mathbf{g}_{\max}} = \begin{bmatrix} 1 \\ \mathtt{M} \\ 1 \end{bmatrix} . \tag{15}$$

In order to achieve this, matrix **S** is modified to obtain a new matrix $\mathbf{T} = [t_{ij}]$, with elements given by

$$t_{ij} = \frac{s_{ij}}{\sum_{j=1}^{p} s_{ij}} . \tag{16}$$

The new approximation is then given by $\boldsymbol{\lambda} \approx \mathbf{T}\mathbf{g}$, and it guarantees that

$$\boldsymbol{\lambda}\big|_{\mathbf{g}_{\max}} = \mathbf{T}\mathbf{g}_{\max} = \begin{bmatrix} 1 \\ \mathtt{M} \\ 1 \end{bmatrix} \tag{17}$$

The above mentioned concepts are illustrated in Figure 3, for a hypothetical case with one dependent and two independent variables, *i.e.*, $p = 1$ and $m = 2$. This allows the approximating hyper-planes to become simple planes in 3-dimensional space.

3.2 A simplified interpretation of the inverse problem

The inverse problem consists in estimating **g** from the knowledge of λ. Pre-multiplying both sides of equation (10) by the transpose of **S**, we have

$$\mathbf{S}^T\boldsymbol{\lambda} \approx \mathbf{S}^T(\mathbf{S}\mathbf{g}) = (\mathbf{S}^T\mathbf{S})\,\mathbf{g} \tag{18}$$

In ECT, $\boldsymbol{S^TS}$ will roughly resemble a scaled $p \times p$ identity matrix (see Figure 4). Therefore, $(\boldsymbol{S^TS})$ g in (18) could be considered as a scaled linear approximation to **g**, here denoted by **g***. Thus we write

$$\mathbf{g}^* \approx \mathbf{S}^T\boldsymbol{\lambda} = \mathbf{X}\boldsymbol{\lambda} \tag{19}$$

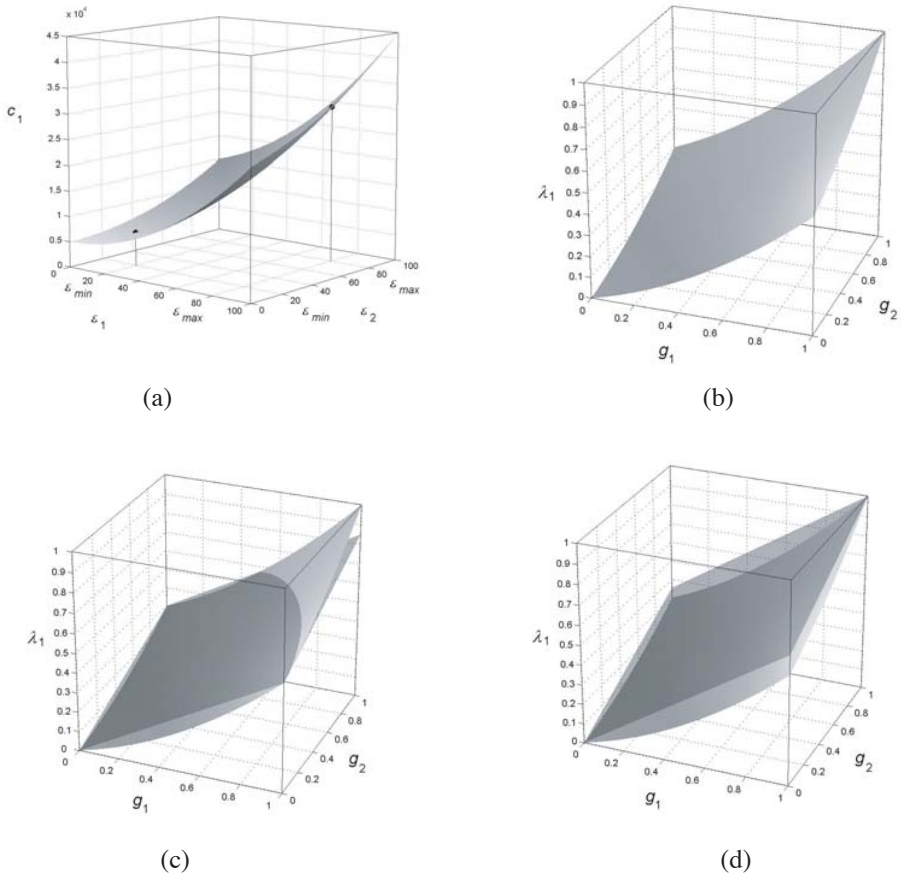

Fig. 3. A hypothetical case with $c_1 = f_1(\varepsilon_1, \varepsilon_2) = 2\,\varepsilon_1^2 + \varepsilon_2^2 + \varepsilon_1\,\varepsilon_2 + 5000$, $\varepsilon_{\min} = 20$ and $\varepsilon_{\max} = 80$. (a) shows the original non-linear function f_1 and (b) the normalised one h_1. The linearised-normalised version is shown in (c) as a superimposed semi-transparent plane (note that it is not an exact approximation for $\mathbf{g} = \mathbf{g}_{\max}$), and (d) shows the re-normalised form.

The size of **X** is $p \times m$. In order to re-gain the correct scale for **g** and so obtain a more realistic approximation, an additional re-normalisation can be introduced, which ensures that

$$\mathbf{g}|_{\boldsymbol{\lambda}_{\mathbf{full}}} = \begin{bmatrix} 1 \\ \mathrm{M} \\ 1 \end{bmatrix} = \mathbf{g}_{\mathbf{max}} \text{ with } \boldsymbol{\lambda}_{\mathbf{full}} = \begin{bmatrix} 1 \\ \mathrm{M} \\ 1 \end{bmatrix} = \mathbf{T}\mathbf{g}_{\mathbf{max}} \ . \quad (20)$$

For this, matrix $\mathbf{X} = [x_{ij}]$ shown in (19) is modified to obtain matrix $\mathbf{R} = [r_{ij}]$, with elements given by

$$r_{ij} = \frac{x_{ij}}{\sum_{j=1}^{m} x_{ij}} \ . \quad (21)$$

The use of this matrix **R** guarantees that

$$\mathbf{g}|_{\boldsymbol{\lambda}_{\mathbf{full}}} = \mathbf{R}\ \boldsymbol{\lambda}_{\mathbf{full}} = \begin{bmatrix} 1 \\ \mathrm{M} \\ 1 \end{bmatrix} . \quad (22)$$

And finally, we arrive to the LBP method

$$\mathbf{g} \approx \mathbf{R}\boldsymbol{\lambda} \ . \quad (23)$$

This is exactly the same as (3). Note that in order to use the LBP method we must know all the $f_i(\varepsilon_j)$, as well as all the $f_i(\boldsymbol{\varepsilon}_{\mathbf{max}})$ and $f_i(\boldsymbol{\varepsilon}_{\mathbf{min}})$, the capacitance measurements for 'full' and 'empty' sensor, respectively. All these data are required to determine the matrix **S**, from which the actual reconstruction matrix **R** is eventually obtained.

4. RESULTS

In order to illustrate the application of the LBP method, we computed the synthetic response for a twelve-electrode ECT sensor. The capacitance values for all single-electrode combinations were calculated. We considered a two-component distribution with a lower permittivity material of 1.0 (air) and a higher permittivity material of 2.5 (oil). We considered three typical oil-flow patterns: annular, stratified and bubbly flows. We added a random noise level of 5% into the capacitance data. Results are shown in Figure 5, and quality of the reconstructed images is not quite good, especially in the case of multiple objects in the image. In general, the reconstructed images resemble the flow phantoms, particularly

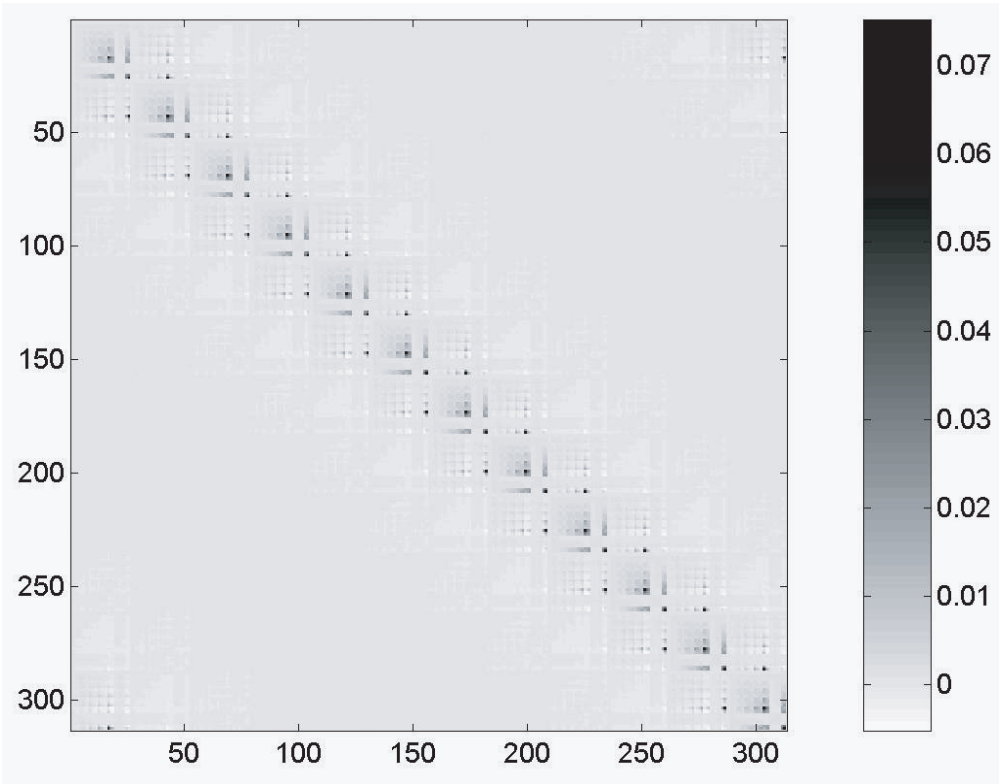

Fig. 4. Image of $\mathbf{S}^T\mathbf{S}$. **S** was assembled from the sensitivity maps calculated for a 12-electrode ECT sensor ($m = 66$), with $p = 313$, $\varepsilon_{min} = 1$ and $\varepsilon_{max} = 2.1$.

for annular and stratified flow patterns. In all cases, the flow type can be identified. Image reconstruction by the LBP method provides low image resolution when small objects (like bubbles) are in the middle of the pipe cross-section. This limitation can be overcome by the use of iterative methods to the cost of much higher computation times.

We also applied the LBP method to real ECT data. We introduced a perspex bar, with permittivity value of 2.1, inside the sensor in two different positions. Location of the object can be easily identified and the shape of the object was nicely approximated by the LBP reconstruction algorithm (see Figure 6). The resolution of the reconstructed image is not high, as in the previous case. Depending on the application, a compromise must be made between the system resolution, accuracy, sensitivity and speed of computation.

As a final part of this work we applied the LBP method to a real gas-oil two-phase flow. The sets of electrical capacitance tomography measurements used in this part of the study were collected in a 3-inch gas-oil two-phase test loop. As we mentioned above, we used a 12-electrode pressure-resistant capacitance tomography sensor.

In this work, we tested a number of flow regimes generated by modifying oil and gas flow rates. We used as a reference a view trough a transparent window section installed in the test loop. Stratified flows can be directly seen through the transparent window but other patterns involving significant gas flows cannot be observed properly in the inner core of the sensor because the oil phase is reflected by the sensor walls and the window. The test loop uses nitrogen gas, Exxol D80 oil and tap water. In this work we only used air and oil as flow components. We used a sensitivity matrix computed for a set of 1693 elements or pixels.

Air and oil were injected through the sensor at different pressures up to 7 barg and at a temperature around 20°C. The velocities of each phase were varied through a pressurized valve system. Ten different flow patterns were generated and sets of measurements, during around 30 seconds, were collected for each pattern.

In Figure 7 we show a set of results for one of the more complex patterns we found: a stratified intermittent flow. As can be seen in this plot, large oscillations of the flow are observed in the snapshots, forming semi-annular patterns close to the sensor wall. The liquid flow rate was increased maintaining the gas flow rate low. An intermittent flow pattern is then observed, with an alternant occurrence of slugs and stratified flows. Sequence of reconstructed images goes from top to bottom and from left to right, and delay time between frames is 50 ms. As the LBP method is a real-time one step reconstruction approach it can easily deal with this speed of data acquisition.

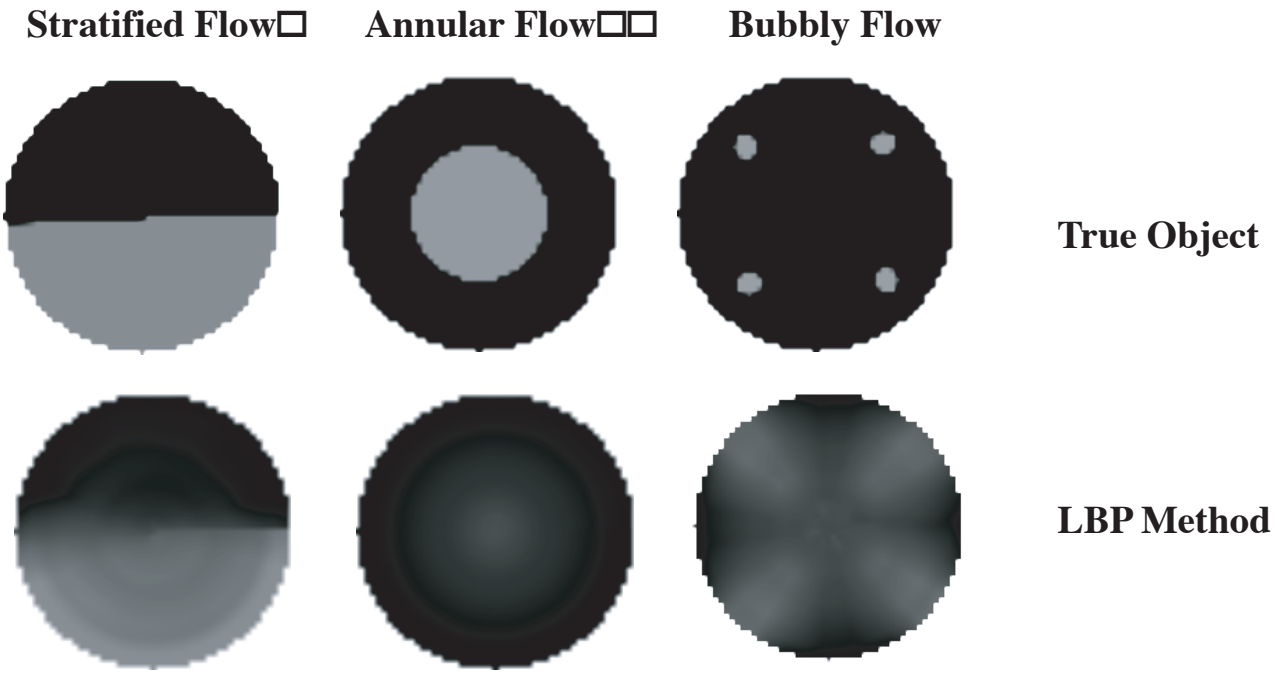

Fig. 5. Image reconstructions for typical synthetic oil-pipe flows by using the LBP method.

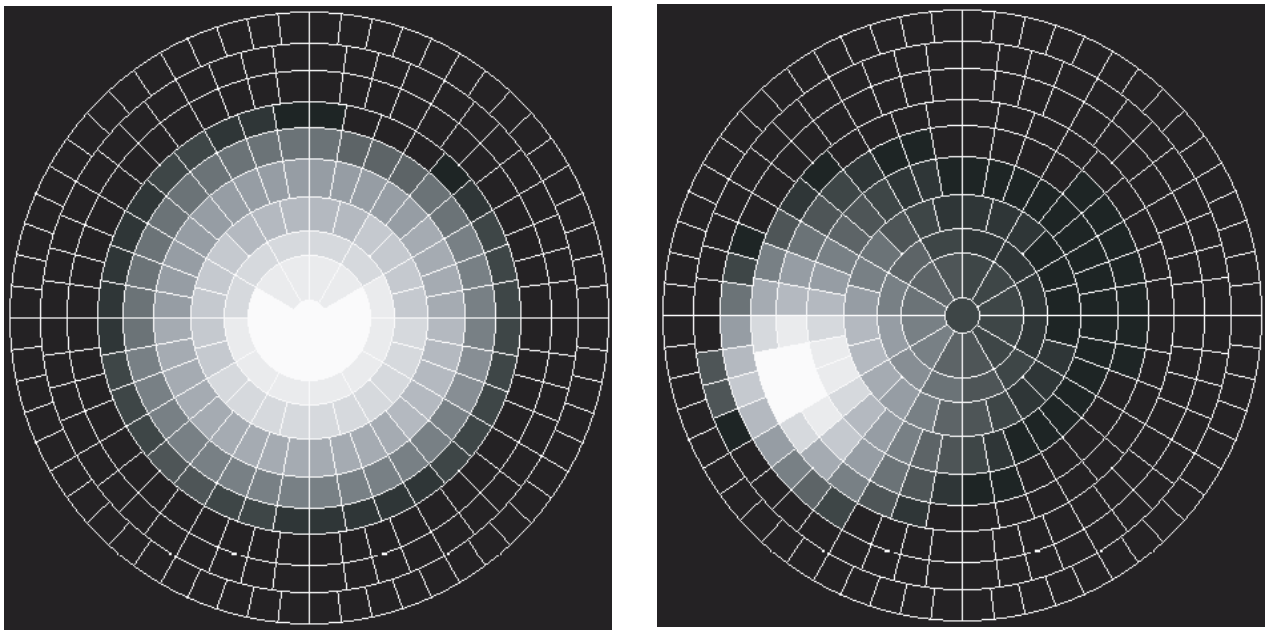

Fig. 6. LBP image reconstructions for real data: a) Perspex bar ($\varepsilon_r = 2.1$) in the center; b) Bar half way between centre and wall.

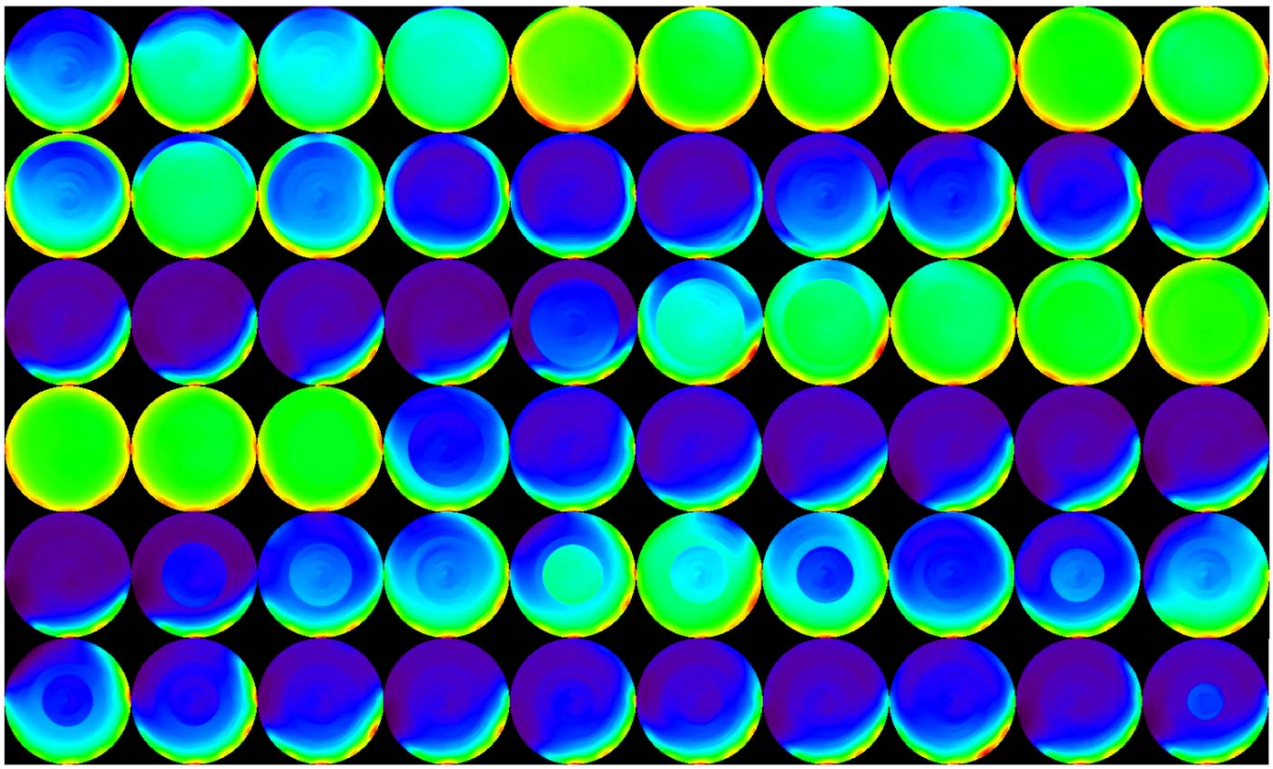

Fig. 7. Image reconstruction of a real gas-oil two-phase intermittent flow. Red represents high permittivity material (oil) and blue represents permittivity of air. Intermediate colours (yellow, green and light blue) are associated to presence of oil in progressively lower concentrations. Sequence goes from top to bottom and from left to right. Delay time between frames is 50 milliseconds.

Visualizations using LBP are limited because half of the image contours are not specifically interfaces; however they give a regular indication of the flow composition. There exists a resolution trouble in the central zone of the sensor where some kind of phantom can be seen in some of the snapshots mainly caused by errors introduced at the normalization stage.

5. CONCLUSIONS

It was shown that LBP is actually based on the linearisation of a normalised form of the original forward problem. More specifically, the normalised forward problem is approximated by means of a series of hyper-planes. The reconstruction matrix used in LBP is a 'weighted' transpose of the linear operator (*i.e.*, matrix **S**) that defines the linearised-normalised forward problem. The rows of **S** contain the information of the sensitivity maps used in LBP. Note that the image-reconstruction errors in LBP for ECT arise basically from (a) the initial linearisation of the forward problem, (b) the fact that $\mathbf{S}^T\mathbf{S}$ actually departs in some degree from a perfect scaled identity matrix, and (c) the final re-normalisation to obtain **R** (albeit this only really 're-distributes' the errors). Reconstructions of synthetic and real data were included, in order to illustrate application of the LBP method to ECT data inversion. We also applied the LBP method to the reconstruction of gas-oil flows from measured ECT data by using a state of the art high-pressure resistant sensor in a test loop facility. As a consequence of this work, the LBP method can be used for routine interpretation of ECT data in two-phase gas-oil flow imaging.

6. BIBLIOGRAPHY

ISAKSEN, O., 1996. A review of reconstruction techniques for capacitance tomography. *Measur. Sci. Tech., 7,* 325-37.

ORTIZ-ALEMÁN, C., R. MARTIN and J. GAMIO, 2004. Reconstruction of permittivity images from capacitance tomography data by using very fast simulated annealing. *Measur. Sci. Tech., 15,* 1382-1390.

XIE, C. G., A. PLASKOWSKI and M. S. BECK, 1989. 8-electrode capacitance system for two component flow identification. Part 1: Tomographic flow imaging. IEE Proceedings A, 136 (4), 173-183

XIE, C. G., S. M. HUANG, B. S. HOYLE, R. THORN, C. LENN, D. SNOWDEN and M. S. BECK, 1992. Electrical capacitance tomography for flow imaging: System model for development of image reconstruction algorithms and design of primary sensors. IEE Proc.-G, 139 (1), 89-98.

YANG, W. Q., M. S. BECK and M. BYARS, 1995. Electrical capacitance tomography: from design to applications. Measur. and Control, 28, 261.

YANG, W. Q. and L. PENG, 2003. Image reconstruction algorithms for electrical capacitance tomography. *Measur. Sci. Tech., 14,* R1-R13.

J. C. Gamio, C. Ortiz-Alemán and R. Martin

Instituto Mexicano del Petróleo
Eje Central Lázaro Cárdenas 152,
07730 México, D. F, México
Email: jgamio@imp.mx